Broadband Arbitrary Waveform Generation Based on Microwave Frequency Upshifting in Optical Fibers

José Azaña, *Member, IEEE*, Naum K. Berger, Boris Levit, and Baruch Fischer

***Abstract*—An interesting method for broadband arbitrary waveform generation is based on the frequency upshifting of a narrowband microwave signal. In this technique, the original microwave signal is imaged into a temporally compressed replica using a simple and practical fiber-based system. Recently, it has been shown that the conventional limitations of this approach (e.g., bandwidth limitations) can be overcome by exploiting a temporal self-imaging (Talbot) effect in fiber. This effect can be used whenever the signal to be imaged is a quasi-periodic waveform (e.g., microwave tones or any arbitrary periodic waveform). This paper provides a comprehensive study of the microwave frequency upshifting technique with special focus on the Talbot-based approach. Following a theoretical analysis of the design constraints of the conventional approach, the Talbot-based solution is theoretically investigated in detail. In particular, the design specifications of a Talbot-based microwave upshifting system are derived, and the practical capabilities and constraints of these systems (e.g., in terms of achievable bandwidth) are stated and examined. The theoretical findings are confirmed by means of numerical simulations. Moreover, a numerical study of the influence of higher-order (second-order) dispersion terms on system performance is presented, and some additional design rules to minimize the associated detrimental effects are given. The results show that microwave frequencies up to a few hundreds of gigahertz over nanosecond temporal windows can be easily obtained with the described technique using input optical bandwidths in the terahertz range. This has been experimentally confirmed.**

***Index Terms*—Arbitrary waveform generation, fiber optics, microwave photonics, optical propagation, optical signal processing, Talbot effect, temporal imaging.**

I. Introduction

THE DEVELOPMENT of novel techniques for the generation, control, and manipulation of high-frequency microwave signals is becoming increasingly important for several scientific and industrial applications, including among others, ultrawide-bandwidth (UWB), secure, and multiple-access radio frequency (RF) communication systems, electronic countermeasures, or pulsed radar and fiber wireless communication systems. The generation of RF radiation (tones) above 40 GHz using conventional methods (electronics) is extremely complex and costly. Moreover, current electromagnetic arbitrary waveform generation (AWG) is limited to the range below ≈ 2 GHz. It is well known that photonically assisted techniques can drastically enhance the performance of electronic systems for the generation and manipulation of microwave signals [1]–[7]. In particular, several photonics-based techniques have been demonstrated for the generation of microwave waveforms in the gigahertz and multiple tens of gigahertz range. For instance, photonic AWG has been demonstrated by individually modulating the intensity and phase of the longitudinal frequency modes of a mode-locked semiconductor laser [3]. Optical and microwave waveforms with arbitrary wideband modulation have also been generated using programmable spectral shaping of a supercontinuum source followed by wavelength-to-time mapping in a dispersive line [4]. It has been shown that conventional optical pulse shaping techniques, such as direct space-to-time optical pulse shaping, can be used for the reconfigurable generation of broadband arbitrary electromagnetic waveforms [6]. The potential of combined dispersion and nonlinear effects in optical fiber systems for generating complex microwave pulses has also been investigated [5]. These optical techniques for microwave generation are generally limited by the bandwidth of the optical receiver [i.e., photodetector (PD)] to operations up to a few tens of gigahertz.

An interesting alternative method for generating broadband microwave signals is based on the frequency upshifting of a narrowband microwave signal (which can be first generated using conventional electronics) [1]. In this technique, the original microwave signal is imaged into a temporally compressed replica by means of a simplified temporal imaging (TI) system (i.e., time lens process followed by dispersion); this system can be practically implemented using an intensity electrooptic (EO) modulator (to transfer the microwave signal into the optical domain) surrounded by two dispersive fibers, in which an ultrashort (ultrabroadband) pulse is used as the optical input (see schematic in Fig. 1). This translates into a very simple and practical system that offers the inherent advantages of a fiber-based solution (compact and robust solution, potential for low cost, etc.). It is important to note that this same system can be configured to implement microwave temporal stretching; in this case, the original microwave signal is imaged into a temporally *stretched* replica at the system output [2]. Temporal stretching can be used for analog-to-digital conversion of wideband microwave signals by slowing down the signal to be captured prior to digitization; using this technique, the effective sampling rate and input bandwidth of a given analog-to-digital converter can be increased in proportion to the time stretch factor.

The main drawback of the microwave frequency upshifting approach in [1] is that in principle, the maximum microwave bandwidth that can be generated with this approach is very limited. This bandwidth limitation is intrinsic to the specific system

Manuscript received October 1, 2005; revised March 23, 2006.

J. Azaña is with the Institut National de la Recherche Scientifique-Énergie, Matériaux et Télécommunications (INRS-EMT), Montreal, QC H5A 1K6, Canada (e-mail: azana@emt.inrs.ca).

N. K. Berger, B. Levit, and B. Fischer are with the Department of Electrical Engineering, Technion—Israel Institute of Technology, Haifa 32000, Israel (e-mail: fischer@ee.technion.ac.il).

Digital Object Identifier 10.1109/JLT.2006.875212

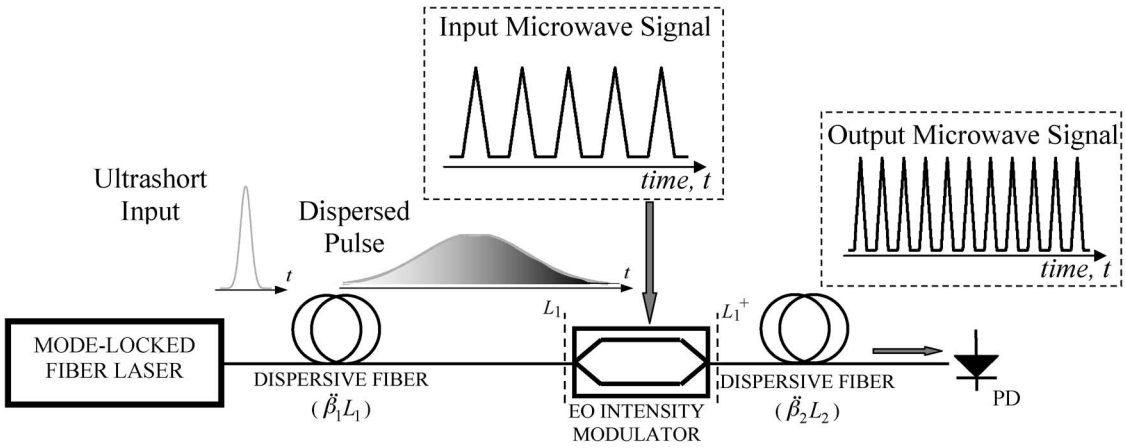

Fig. 1. Schematic of the fiber-based microwave frequency upshifting technique.

configuration for obtaining TI [2], [8]. Briefly, as compared with an ideal TI system (dispersion + time lens + dispersion) [9], a simplified TI system (time lens + dispersion) leads to a *nonfocused* image in time. A nonfocused image manifests itself as a classical dispersion where slow phenomena appear clearly but fast phenomenas (high frequencies) are filtered out. This nonfocused imaging process is essentially responsible for the anticipated limitation in the maximum microwave frequency that can be handled (e.g., generated) by a simplified TI system. As an example, the maximum RF frequency that could be generated with the system demonstrated in [1] was 25 GHz (starting from a 10-GHz tone), although an input optical source with an ultrabroadband bandwidth of ≈ 4 THz was employed.

The dispersion penalty in a simplified TI system is qualitatively similar to that occurring in analog fiber links [8]. Based on this similarity, it has been shown that this penalty (and the associated bandwidth limitation) can be minimized by employing optical single-sideband (SSB) intensity modulation instead of the conventional optical double-sideband (DSB) modulation scheme [10]. In a simplified TI system, optical SSB should be implemented using phase discrimination methods, which require the use of a double-arm Mach–Zehnder modulator. Obviously, this translates into a significantly increased complexity in the EO modulation scheme. Another important drawback of the SSB modulation technique is that it introduces an additional nonlinear phase distortion, which is especially detrimental when used over a broad bandwidth (such as in the case of our application); this also limits the microwave bandwidth over which these systems can be applied in practice.

More recently, we have demonstrated that the typical bandwidth limitation in a simplified TI system (based on conventional DSB modulation) can be easily overcome by exploiting a temporal self-imaging (Talbot) effect in the optical fiber [7]. This effect can be used whenever the microwave signal to be temporally imaged (compressed) is an *arbitrary* periodic RF signal (e.g., microwave tones). By using the temporal Talbot effect, a similar configuration to that used for a nonideal simplified TI (time lens + dispersion) can be used to create a TI system that leads to a *focused* image of the original event (i.e., like in an ideal TI system). In this way, the typical dispersion penalty in these systems is significantly reduced, and in fact, it has been shown that the Talbot-based approach provides an unparalleled design flexibility to achieve a desired frequency upshifting. In particular, based on this approach, microwave tones of around 50 GHz have been generated from $\approx$ 10-GHz tones using a relatively modest input optical bandwidth (of order of 1 THz) [7]. The superior capabilities provided by the Talbot-based microwave frequency upshifting technique have been further demonstrated by upshifting $\approx$ 40-GHz microwave tones to achieve optical temporal waveforms (sinusoidal envelopes) above 350 GHz [7].

This paper provides a comprehensive study of the microwave frequency upshifting technique [1], [7]. The principle of operation of the conventional approach [1] is first investigated in detail (Section II); in particular, the equations governing a conventional microwave frequency upshifting system are derived, from which the main limitations of this approach (e.g., in terms of achievable bandwidth) are deduced and discussed. The main core of our paper is the theoretical analysis of the Talbot-based microwave frequency upshifting method (Section III). The principle of operation of this method is described in detail and the design specifications of a Talbot-based system for frequency upshifting are derived. Based on these results, the practical capabilities and constraints of these systems (e.g., in terms of achievable microwave bandwidth) are clearly stated and examined. Our analysis shows the superior performance offered by a microwave frequency upshifting system when configured to exploit the temporal Talbot effect. Moreover, we show that the Talbot-based approach is not restricted to strictly periodic RF signals but can also be applied on quasi-periodic temporal waveforms, such as slowly (amplitude and/or phase) modulated microwave tones. The design constraints of a Talbot-based frequency upshifting system for operating on quasi-periodic temporal waveforms are also derived here. Numerical simulations are provided to illustrate the Talbot-based frequency upshifting approach, thus confirming our main theoretical findings (Section IV). Moreover, a numerical investigation of the influence of higher order (second-order) dispersion terms on system performance is presented and some additional design specifications are derived from this investigation. For completeness, in Section V, we describe in detail our previously reported

proof-of-concept experiments on the Talbot-based microwave frequency upshifting method. We summarize and conclude our work in Section VI.

II. Fiber-Based Microwave Frequency Upshifting

A. Operation Principle

The concept of microwave frequency upshifting is based on imaging a given low-frequency microwave waveform (which can be generated by conventional electronic methods) into a temporally compressed replica. This TI process can be achieved by using the simple fiber-based system shown in Fig. 1. An ultrashort optical pulse is first dispersed in a dispersive element (e.g., optical fiber), which introduces a total dispersion $\ddot{\beta}_1 L_1$, where $\ddot{\beta}_1$ is the first-order dispersion coefficient of the fiber, $\ddot{\beta}_1 = [\partial^2 \beta_1(\omega)/\partial\omega^2]_{\omega=\omega_0}$ ($\beta_1(\omega)$ is the fiber propagation constant as a function of the optical angular frequency ω, and ω_0 is the pulse's central frequency), and L_1 is the fiber length. The dispersed optical pulse is temporally modulated by the input electrical (microwave) signal using an intensity EO modulator. In this way, the microwave waveform is transferred into the optical domain; moreover, the linear chirp (quadratic phase) of the optical pulse after dispersion is imposed onto the microwave signal. This mechanism of quadratic phase modulation (PM) of the temporal microwave waveform can be interpreted as a time lens [9]. The so-called temporal aperture of the system (temporal window over which the TI system operates) is thus determined by the temporal duration of the chirped optical pulse at the output of the first dispersive line. A temporally compressed replica of the amplitude waveform at the output of the EO modulator (which in turn is proportional to the input microwave waveform) can be obtained by simply propagating this signal through a second dispersive line (e.g., optical fiber) with a dispersion of opposite sign to that at the input. This operation is usually referred to as TI [2], [9]. The signal is finally transformed back into the electronic domain using a PD operating as an optical-to-electrical converter.

To understand and analyze the TI system in Fig. 1, we assume an ultrashort Gaussian pulse as the optical input to the system. After propagation through the first dispersive line (optical fiber) of length $L1$, this pulse is temporally broadened and chirped. In particular, assuming that the input dispersion is sufficiently high, the complex envelope of the pulse at the fiber output can be expressed as

$$u\left(t, L_1^-\right) = \exp\left(-\left(\frac{t}{\tau_1}\right)^2\right) \exp\left(j\frac{t^2}{2\ddot{\beta}_1 L_1}\right) \tag{1}$$

with $\tau_1 \approx \ddot{\beta}_1 L_1 \Delta\omega_{\text{opt}}$, where $\Delta\omega_{\text{opt}}$ is the input optical bandwidth. Notice that in our analysis the time delays introduced by the different elements in the system (i.e., dispersions and EO modulator) are not considered. The chirped pulse is then intensity modulated in an EO modulator (e.g., Mach–Zehnder intensity modulator) by an arbitrary electrical (microwave) signal $V_{\text{in}}(t)$. The modulation depth is assumed to be sufficiently small to ensure a linear modulation operation. In this way, the electrical waveform is transferred into the optical domain. In particular, the optical signal at the output of the EO modulator can be written as [2]

$$u\left(t, L_1^+\right) = u\left(t, L_1^-\right)\left[1 + aV_{\text{in}}(t)\right] = V'(t)\exp\left(j\frac{t^2}{2\ddot{\beta}_1 L_1}\right) \tag{2}$$

where $V'(t) = \exp(-[t/\tau_1]^2)[1 + aV_{\text{in}}(t)]$. The expression in (2) is valid as long as the modulation depth is sufficiently small, i.e., $a \ll 1$. The time duration of the chirped optical pulse τ_1 determines the temporal window over which the input signals (to be temporally imaged) can extend. This is the so-called temporal aperture of the system and is essentially determined by the input dispersion and input optical bandwidth (see above expression). The optical signal at the output of the EO modulator is dispersed again in a second dispersive line (optical fiber) providing a total dispersion $\ddot{\beta}_2 L_2$. As mathematically demonstrated in the Appendix, if the spectral bandwidth of the signal $V'(t)$ is sufficiently narrow, then the optical signal at the output of the second dispersive line can be expressed as

$$u(t, L_1 + L_2) \propto \exp\left(j\frac{t^2}{2(\ddot{\beta}_1 L_1)M_t}\right) V'\left(\tau = \frac{t}{M_t}\right) \tag{3}$$

where M_t is the so-called temporal magnification factor, which depends on the ratio between the output and the input dispersions in the system, i.e.,

$$M_t = 1 + \frac{\ddot{\beta}_2 L_2}{\ddot{\beta}_1 L_1}. \tag{4}$$

The signal received at the output of the PD $V_{\text{out}}(t)$ is proportional to the average intensity of the optical signal at its input, and as a result

$$\begin{aligned} V_{\text{out}}(t) &\propto |u(t, L_1 + L_2)|^2 \propto \left|V'\left(\tau = \frac{t}{M_t}\right)\right|^2 \\ &\approx \exp\left(-2\left(\frac{t}{M_t\tau_1}\right)^2\right)\left[1 + 2aV_{\text{in}}\left(\frac{t}{M_t}\right)\right]. \end{aligned} \tag{5}$$

Thus, under proper conditions, the output electrical signal is a magnified or compressed temporal replica of the input electrical signal with a time magnification factor M_t given by (4). In order to achieve temporal compression (i.e., frequency upshifting), the TI system must be configured so that $|M_t| < 1$, and as a result, the two dispersive lines in the system must provide dispersions with opposite signs; see (4). In contrast, temporal stretching of the original microwave waveform can be achieved if the two dispersive lines have the same dispersion sign [2]. Notice that at the system output, the compressed (or magnified) replica of the input temporal waveform is modulated in amplitude by a slow Gaussian temporal envelope over a total duration equal to the input temporal aperture (τ_1) multiplied by the time magnification factor of the system. Moreover, the signal exhibits a dc background determined by this same Gaussian temporal function.

B. Bandwidth Limitations

According to the derivations in the Appendix, in order to ensure that the output electrical signal is a temporal image of the input electrical signal, the following inequality must be satisfied:

$$|\alpha|\frac{\Delta\Omega^2}{8} \ll \pi \tag{6}$$

where $\Delta\Omega$ is the total spectral bandwidth of $V'(t)$ and $1/\alpha = (1/\ddot{\beta}_1 L_1) + (1/\ddot{\beta}_2 L_2)$. Inequality (6) implies that the time features of bandwidth $\Delta\Omega$ will almost not be distorted by propagation through a dispersive medium introducing a total dispersion equal to α.

The condition in inequality (6) imposes a fundamental limitation in the maximum output electrical bandwidth that can be generated with the described system. To be more concrete, inequality (6) can be conveniently rewritten as

$$\Delta\omega_{\rm in}^2 \ll 2\pi\frac{|M_t|}{|\ddot{\beta}_2 L_2|} \tag{7}$$

where $\Delta\omega_{\rm in}$ is the spectral bandwidth of the input microwave signal. For instance, if the input signal is an electrical tone of frequency ω_m, i.e., $V(t) = A\cos(\omega_m t + \phi)$, then $\Delta\omega_{\rm in} = \omega_m$. In deriving (7), we have assumed that the input microwave signal is much faster than the slow Gaussian temporal envelope that modulates this signal when transferred to the optical domain, i.e., $\Delta\omega_{\rm in} \gg 2\pi/\tau_1$; in this case, $\Delta\Omega \approx 2\Delta\omega_{\rm in}$. The microwave frequency shifting operation can thus be interpreted as a low-pass filtering process with a bandwidth constrained by (7). This bandwidth can be increased *only* by reducing the amount of dispersion in the second dispersive element, which requires reducing the dispersion introduced by the first dispersive element (in order to keep the same temporal magnification factor). However, a reduction in the input dispersion directly translates into a reduction of the temporal aperture of the system. This fundamental tradeoff between the microwave bandwidth and the temporal aperture in a simplified TI system essentially determines the poor performance of this system in terms of the maximum frequency that it can handle in practice [10]. To be more concrete, assuming that the system is configured to obtain a high temporal compression, i.e., $|M_t| \ll 1$, then $|\ddot{\beta}_2 L_2| = |\ddot{\beta}_1 L_1||M_t - 1| \approx |\ddot{\beta}_1 L_1|$, and as a result, (7) can be rewritten as

$$\tau_1\Delta\omega_{\rm in} \ll 2\pi\frac{\Delta\omega_{\rm opt}}{\Delta\omega_{\rm out}} \tag{8}$$

where $\Delta\omega_{\rm out} \approx \Delta\omega_{\rm in}/|M_t|$ is the bandwidth of the compressed electrical signal (i.e., at the output of the system), and we recall that $\tau_1 \approx |\ddot{\beta}_1 L_1|\Delta\omega_{\rm opt}$ is the system's temporal aperture. Thus, the time–bandwidth product of the system (in which time refers to the input temporal aperture) is constrained according to (8): A higher output frequency can be achieved *only* by decreasing the system time–bandwidth product. Notice that basically, the time–bandwidth product determines the number of temporal features (of resolution $\delta\tau \approx 2\pi/\Delta\omega_{\rm in}$) in the input signal that can be imaged with a given system configuration. To give reference, according to inequality (8), the maximum microwave bandwidth that can be achieved with a given system configuration is about one order of magnitude narrower than the input optical bandwidth; in this case ($\Delta\omega_{\rm out} \approx \Delta\omega_{\rm opt}/10$), the time–bandwidth product is limited to $\tau_1\Delta\omega_1 \approx 2\pi$, which means that only a *single* temporal feature can be imaged! As a practical example, the maximum RF frequency that could be generated with the system configuration in [1] was $\approx$ 25 GHz (from a 10-GHz input tone) for an input temporal aperture of $\approx$ 2 ns, corresponding to a time–bandwidth product of $\approx$ 20.

In general, a microwave frequency upshifting system is restricted to waveform generation over a limited time window. Nonetheless, it should be emphasized that the generation of time-limited broadband arbitrary waveforms is still highly desired for many important applications, including UWB code-division multiple-access (CDMA) systems, pulsed radar and testing of communication receivers [4]–[6], among others.

III. Frequency Upshifting of Periodic Microwave Waveforms Using Temporal Self-Imaging in Optical Fibers

The described constraints of a frequency upshifting system operating on electrical waveforms can be significantly overcome by exploiting a temporal self-imaging (Talbot) effect in optical fibers [11]. Using this effect, one can achieve a *focused* compressed (or magnified) temporal image of an *arbitrary periodic microwave temporal waveform* by use of the same simplified TI system (shown in Fig. 1) [8]. This so-called general temporal self-imaging effect can be interpreted as the time-domain equivalent of the well-known spatial self-imaging (Talbot) effect *under point source illumination* [11]. We emphasize that in order to exploit the Talbot effect, the input microwave signal must be a (quasi-)periodic temporal waveform. This includes nonmodulated or slowly (amplitude and/or phase) modulated microwave tones (sinusoidal waveforms), or in general, any given arbitrary periodic waveform. In what follows, the design specifications of the Talbot-based approach for the frequency upshifting of (quasi-)periodic microwave waveforms will be derived, and the superior performance provided by this approach as compared with the conventional one will be discussed.

A. Operation Principle

Let us now assume that the input microwave signal $V_{\rm in}(t)$ is a periodic temporal waveform of repetition period T_m (repetition frequency $\omega_m = 2\pi/T_m$). With reference to Fig. 1, the optical signal at the output of the EO intensity modulator can be expressed as in (2), in which $V'(t) = \exp(-[t/\tau_1]^2)[1 + aV_{\rm in}(t)]$ consists of a periodic waveform (of period T_m) modulated by a slow temporal Gaussian envelope. The problem under consideration can be analyzed as follows: the quasi-periodic optical waveform $V'(t)$ is first phase-modulated by a linear chirp function $\exp(jt^2/2\ddot{\beta}_1 L_1)$ (temporal phase chirp $\dot{\phi}_t = 1/\ddot{\beta}_1 L_1$) and then propagates through a first-order dispersive medium (e.g., optical fiber), which introduces a total dispersion $\ddot{\Phi}_\omega = -\ddot{\beta}_2 L_2$. This same problem was investigated in [11], and

general temporal self-imaging phenomena were anticipated. In this paper, we will not replicate the mathematical details of the analysis of this problem; rather, we will focus on the relevant results for our specific application. It should be noted that the proposal in [11] was oriented to processing optical waveforms (instead of electrical waveforms, as in our application here). This translates into a different implementation for the time lens process (linear chirp temporal modulation). Different alternatives exist for implementing a time lens over an optical waveform, including EO PM [12] and sum–frequency generation in a nonlinear crystal [13]. The implementation of a time lens process on a microwave waveform is relatively simpler. As described above, this process can be realized by simply modulating a chirped optical pulse with the microwave signal to be processed in an EO intensity modulator, thus imposing the optical linear chirp $\ddot{\phi}_t = 1/\ddot{\beta}_1 L_1$ along the electrical temporal waveform.

According to the analysis in [11], a temporal image of the quasi-periodic optical waveform $V'(t)$ can always be obtained at the output of the system if the time lens process and dispersive line in the system are properly designed to induce a temporal self-imaging process, i.e., the so-called *integer* self-imaging or Talbot condition must be satisfied. To be more concrete, if this Talbot condition is satisfied, the electrical signal at the output of our system (output of the PD) can be expressed as in (5) with a temporal magnification factor M_t also given by (4). As mentioned above, temporal compression (i.e., frequency upshifting) can be achieved if the input and output dispersive lines provide dispersions with opposite signs. The so-called *integer* Talbot condition can be written as [11]

$$|\ddot{\beta}_2 L_2| = N\frac{T_m^2}{2\pi}|M_t| \tag{9}$$

where N is an *arbitrary positive integer* $(N = 1, 2, 3, \ldots)$. This condition is strictly valid if the input signal is an ideal periodic waveform.

In our case, the input signal $V'(t)$ is a quasi-periodic waveform, i.e., a periodic waveform of temporal period T_m, modulated by a slow Gaussian temporal envelope of duration τ_1. The problem of general self-imaging of a periodic waveform modulated by a duration-limited slow temporal envelope has also been investigated in [11]. In particular, it has been demonstrated that the temporal aberrations induced by the time-limited temporal envelope on the output waveform (as compared with the ideal temporal image of the input waveform) are negligible if this temporal envelope is sufficiently slow to satisfy the inequality ([11, eq. (40)])

$$\Delta\omega_{\text{env}} \ll 2\pi\frac{\Delta t_0}{NT_m^2} \tag{10}$$

where $\Delta\omega_{\text{env}}$ is the spectral bandwidth of the temporal envelope and Δt_0 is the temporal duration of the periodic waveform within a single period. In our analysis, the temporal envelope is a Gaussian function, and as a result, the envelope's bandwidth can be estimated as $\Delta\omega_{\text{env}} \approx 2\pi/\tau_1$. For simplicity, we will consider the temporal duration of the electrical waveform within each period to coincide with the temporal period itself (for instance, this is the case of a sinusoidal waveform), i.e., $\Delta t_0 \approx T_m$. Introducing these two approximations into (10), we finally derive the condition

$$\tau_1 \gg NT_m. \tag{11}$$

Inequality (11) implies that the temporal duration of the stretched optical pulse at the output of the first dispersive line must be much larger than N times the period of the electrical waveform to be imaged. In the following sections, the design constraints imposed by the derived conditions for frequency upshifting of periodic and quasi-periodic electrical waveforms will be analyzed in detail.

B. Design Specifications for Frequency Upshifting of Periodic Microwave Waveforms

The main design equation for the frequency upshifting of periodic microwave waveforms is the so-called general self-imaging or Talbot condition, i.e., (9). In principle, according to this equation, the output dispersion in the system can be made arbitrarily large. This is associated with the fact that there is a free parameter (N) in (9) that can be fixed at the designer convenience, i.e., the output dispersion can be made larger by simply fixing a higher value for the free parameter N. In this way, the system's input dispersion [which is directly proportional to the output dispersion for a prescribed time magnification factor; see (4)] can also be made arbitrarily large, and as a result, the temporal aperture of the system $\tau_1 \approx |\ddot{\beta}_1 L_1|\Delta\omega_{opt}$ can be fixed as long as desired, independently of the input (and output) electrical bandwidth in the system. Thus, *the two key performance parameters in the system, namely 1) time aperture; and 2) electrical bandwidth, can be freely optimized as independent parameters*, and as a result, the undesired time–bandwidth tradeoff of the conventional approach can be overcome.

A second design constraint in the system is that given by inequality (11). In reality, condition (11) ensures that the deviations induced by the finite temporal envelope as compared with the ideal case keep within safe bounds [11]. According to condition (11), fixing a higher value of N requires a longer temporal aperture, which is fully consistent with the tendency imposed by the self-imaging condition in (9) (see discussions above).

Inequality (11), in combination with the self-imaging condition (9), however, imposes a constraint on the maximum electrical bandwidth that can be achieved at the output of the system. To be more concrete, assuming that the system is configured to obtain a very high temporal compression, i.e., $|M_t| \ll 1(|\ddot{\beta}_2 L_2| \approx |\ddot{\beta}_1 L_1|)$, the system temporal aperture can be approximated by

$$\tau_1 \approx |\ddot{\beta}_2 L_2|\Delta\omega_{\text{opt}} \approx N\frac{T_m^2}{2\pi}|M_t|\Delta\omega_{\text{opt}} \tag{12}$$

where we have made use of the self-imaging condition in (9). Introducing (12) into inequality (11), we have

$$\frac{T_m}{2\pi}|M_t|\Delta\omega_{\text{opt}} \gg 1. \tag{13}$$

In the case of a sinusoidal waveform, inequality (13) reduces to a simple condition for the output electrical bandwidth $\Delta\omega_{\rm out} \approx \Delta\omega_{\rm in}/|M_t| = 2\pi/(T_m|M_t|)$, and in particular

$$\Delta\omega_{\rm out} \ll \Delta\omega_{\rm opt}. \tag{14}$$

In general, condition (14) means that the maximum electrical bandwidth that can be achieved with the proposed frequency upshifting system is only limited by the input optical bandwidth (without any additional constraint on the system's temporal aperture); specifically, the maximum achievable electrical bandwidth must be much narrower than the input optical bandwidth. Thus, electrical (microwave) frequencies up to a few hundreds of gigahertz could be easily obtained with the proposed technique using pulsed optical sources providing optical bandwidths in the terahertz range. Such optical sources are readily available in different platforms, including optical fiber. One should also keep in mind that in practice, the achievable electrical bandwidth may be limited by the PD bandwidth. Commercially available PDs are limited to bandwidths of about 60 GHz. PD technologies able to handle bandwidths above 300 GHz have been recently reported [14].

It is also worth mentioning that in the analysis presented above, ideal first-order dispersive fibers have been assumed. However, the presence of higher order dispersion terms, and in particular, second-order dispersion terms, may also represent a source of distortion in the analyzed system. The influence of second-order dispersion on the performance of a Talbot-based microwave frequency upshifting system is numerically investigated in Section IV.

C. Design Specifications for Frequency Upshifting of Quasi-Periodic Microwave Waveforms

A problem of relevance from a practical viewpoint is that of frequency upshifting of a periodic microwave waveform modulated by a slow amplitude and/or phase temporal envelope. This includes cases of amplitude-modulated and phase-modulated sinusoidal waveforms, e.g., $V_{\rm in}(t) = A(t)\cos(\omega_m t + \varphi(t))$. The problem is identical to the one analyzed above but in which the input signal exhibits an additional AM/PM. Again, the system must be designed to satisfy the self-imaging condition in (9), as well as to minimize the temporal aberrations induced by the finite-duration amplitude/phase temporal envelope affecting the ideal periodic waveform. Thus, inequality (10) must be also satisfied. Assuming that the amplitude/phase modulation in the electrical waveform is much faster than the slow Gaussian temporal envelope imposed onto the electrical waveform by the stretched optical pulse, i.e., $\Delta\omega_{\rm mod} \gg 2\pi/\tau_1$ ($\Delta\omega_{\rm mod}$ is the bandwidth of the amplitude/phase modulation), then the bandwidth of the temporal envelope that affects the ideal periodic waveform is essentially determined by the modulation bandwidth, i.e., $\Delta\omega_{\rm env} \approx \Delta\omega_{\rm mod}$. Equation (10) can thus be rewritten as

$$\Delta\omega_{\rm mod} \ll \frac{\omega_m}{N} \tag{15}$$

where we have used that $\Delta t_0 \approx T_m$ (sinusoidal waveform). Inequality (15) is a condition for the modulation speed, which must be at least N times slower than the repetition frequency of the input signal. Thus, general self-imaging can also be exploited for the frequency upshifting of amplitude/phase modulated sinusoidal waveforms, but it should be emphasized that this approach can be used for imaging only sufficiently slow temporal modulations. In fact, there is an important tradeoff between the system temporal aperture and the modulation speed; in particular, a longer temporal aperture (higher N) necessarily implies a slower temporal modulation. This is a fundamental limitation in the design of the proposed systems for frequency upshifting of amplitude/phase modulated waveforms.

IV. Numerical Analysis of the Talbot-Based Microwave Frequency Upshifting Approach

A. Design Specifications and Bandwidth Constraints

Our theoretical predictions were confirmed by numerical simulations. As an example, the results of one of our simulated systems are summarized in Fig. 2. Specifically, in this system, the input and output dispersions were fixed to $\ddot{\beta}_1 L_1 = +2000$ ps^2 and $\ddot{\beta}_2 L_2 = -1600$ ps^2, respectively, to achieve a temporal magnification factor of $M_t = 1/5$ (i.e., temporal compression by a factor of 5). Assuming an input optical bandwidth of $\Delta\omega_{\rm opt}/2\pi \approx 1$ THz (estimated *total* bandwidth in our simulations), the temporal aperture at the input of the system is $\tau_1 \approx 12$ ns. The input microwave signal in the presented simulations was an amplitude-normalized periodic train of *triangular* waveforms, each one with a time duration of $\Delta t_0 = 75$ ps. The system output was evaluated for different input repetition frequencies (ranging from $f_m \approx 4$ GHz to $f_m \approx 11$ GHz). In order to illustrate the process of formation of compressed temporal self-images of the input microwave waveform, the cross-correlation coefficient between the normalized output and input microwave waveforms (after proper temporal re-scaling) was calculated for different input repetition frequencies, covering the aforementioned range. This cross-correlation coefficient provides an estimate of the degree of recurrence or similarity between the output microwave waveform and the temporally scaled version (by $1/M_t = 5$) of the input microwave waveform, and in particular, it was computed as

$$C = \frac{\int_{-\infty}^{+\infty} V_{\rm in}(t/M_t)V_{\rm out}(t)dt}{\sqrt{\int_{-\infty}^{+\infty} V_{\rm in}^2(t/M_t)dt \int_{-\infty}^{+\infty} V_{\rm out}^2(t)dt}} \tag{16}$$

where 1) the function $V_{\rm out}(t)$ is background free and normalized in amplitude, and 2) the two functions $V_{\rm in}(t/M_t)$ and $V_{\rm out}(t)$ are temporally synchronized before the computation of this coefficient. Notice that the coefficient C can vary from 0 to 1, and 1 is reached only if $V_{\rm out}(t) = V_{\rm in}(t/M_t)$. As expected, it is observed that the cross-correlation coefficient is maximized (i.e., the output electrical waveform is a compressed replica of the input waveform) for repetition frequencies that satisfy the self-imaging condition in (9) for any given integer N. As anticipated, very high frequencies can be processed using a large value of N without affecting the system's temporal aperture. The insets in Fig. 2 show the simulated input and

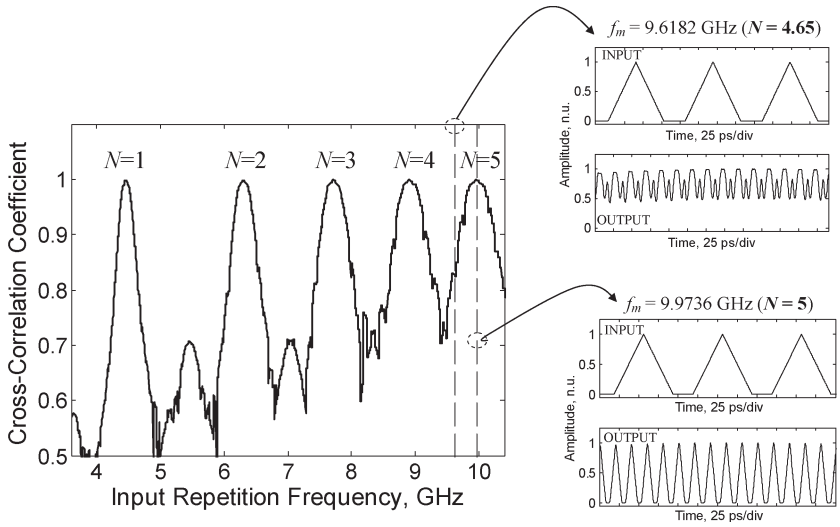

Fig. 2. Results from numerical simulations of a microwave frequency upshifting system, with the parameters given in the text. Cross-correlation coefficient between the output microwave waveform and the temporally compressed replica (by a compression factor of $1/M_t = 5$) of the input microwave waveform (periodic train of triangular signals) evaluated for different input repetition frequencies. Insets show the input and output temporal waveforms for two different input repetition frequencies, namely 1) for $f_m = 9.9736$ GHz, which satisfies the self-imaging condition, and 2) for $f_m = 9.6182$ GHz, which is outside self-imaging conditions.

output temporal waveforms (background-free, normalized waveforms) for two different input repetition frequencies, namely, for $f_m = 9.9736$ GHz, which satisfies the self-imaging condition with $N = 5$, and for $f_m = 9.6182$ GHz, which satisfies (9) with a noninteger N ($N = 4.65$). As shown in this latter example, a significant distortion can be induced in the output waveform if the self-imaging condition is not satisfied.

It has been previously shown that the electrical power transfer function (dispersion-induced power penalty versus RF frequency) of a time-stretched system (or simplified TI system, in general) can be described by a curve that resembles the cross-correlation function in Fig. 2 [8], [10]. The dispersion-induced power penalty function in a time-stretched system is in turn qualitatively similar to that in a conventional RF fiber-optic link [8], [10]. The electrical power transfer function in an RF fiber-optic link (or in a simplified TI system) is calculated for RF tones of different frequencies, and one should keep in mind that in reality, an RF tone is just a particular case of periodic microwave waveforms. In this way, the well-known dispersion-induced power penalty curve in an RF fiber-optic link can be directly related to the temporal Talbot effect in dispersive media. This interpretation is indeed in very good agreement with the conventional one, in which the power penalty curve in an RF fiber link is explained as a result of the dispersion-induced constructive/destructive interference between the carrier–sideband beat terms related to the two sidebands of the modulated signal [10]. The temporal Talbot effect can be similarly explained as a result of dispersion-induced interference between the discrete spectral components of the propagating periodic waveform [15]. In other words, our analysis here reveals that the well-known dispersion-induced power penalty curve in an RF fiber-optic link (and in particular, in a simplified TI system) is not restricted to microwave tones but a similar behavior is also obtained for any given *arbitrary* periodic microwave waveform (where the repetition frequency of the periodic signal plays the role of the RF tone frequency).

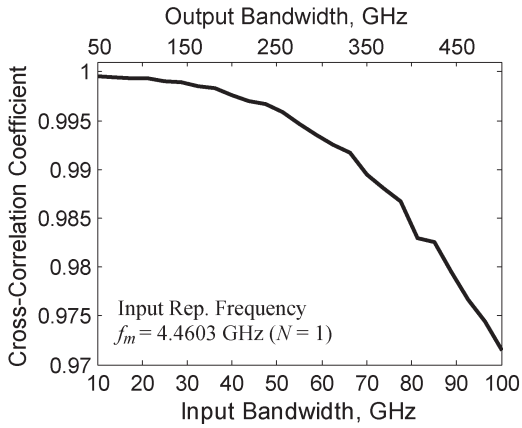

Fig. 3. Results from numerical simulations of the same microwave frequency upshifting system as in Fig. 2. Cross-correlation coefficient between the output microwave waveform and the temporally compressed replica of the input microwave waveform (periodic train of triangular signals) evaluated for different input (output) microwave bandwidths. Bandwidth was varied by changing the time width of the individual triangular pulses. Input repetition frequency was fixed to $f_m = 4.4603$ GHz, which satisfies the self-imaging condition with $N = 1$.

In fact, our proposal for microwave frequency upshifting is based on exploiting this *general* power-penalty feature of a simplified TI system.

In Fig. 3, the cross-correlation coefficient between the output waveform and the temporally compressed replica of the input waveform was evaluated for different input (output) microwave bandwidths. The evaluated system was identical to that simulated in Fig. 2, and in particular, in these present simulations, the repetition frequency of the input microwave signal (train of triangular pulses) was fixed to $f_m = 4.4603$ GHz, which satisfies the self-imaging condition in (9) with $N = 1$. The bandwidth of this input signal was varied by changing the time width of the individual triangular pulses in the sequence. The bandwidth is calculated as half the width of the main lobe of

the spectrum of each triangular pulse (i.e., $\Delta\omega_{\rm in} = 2/\Delta t_0$, where Δt_0 is the time width of each individual triangular pulse). In our simulations, the input microwave bandwidth was varied from 10 to 100 GHz, corresponding to an output microwave bandwidth variation from 50 to 500 GHz (the bandwidth is assumed to increase from the input to the output by exactly the time compression factor of $1/M_t = 5$). As expected, the deviation between the output waveform and the ideally compressed replica of the input waveform is more significant for a broader input (output) bandwidth. The negative slope of the obtained cross-correlation curve becomes notably more pronounced for output bandwidths broader than $\approx$ 200 GHz. This behavior is in good agreement with the above theoretical predictions regarding the system's microwave bandwidth constraints, and in particular, with (14) (we remind the reader that the total optical bandwidth in our simulations was $\approx$ 1 THz).

B. Second-Order Dispersion Effects

The influence of second-order dispersion terms in dispersive fibers on system performance was also numerically investigated. For this purpose, the cross-correlation coefficient between the output waveform and the compressed input waveform was used again. As a general rule of thumb, we expect that the influence of higher order dispersions can be neglected if the dispersive fibers are shorter than the second-order dispersion length L_D corresponding to the input optical bandwidth, i.e., $L_D \approx \delta t_{\rm opt}^3/|\ddot{\beta}_0|$, where $\delta t_{\rm opt} = 2\pi/\Delta\omega_{\rm opt}$, and $\ddot{\beta}_0$ is the second-order dispersion coefficient of the corresponding fiber (at the operation optical wavelength). Based on these preliminary predictions, the cross-correlation coefficients were calculated as a function of a second-order dispersion normalized with respect to the second-order dispersion length (for the used optical bandwidth); in particular, the normalized second-order dispersion was defined as $|\dddot{\beta}_0|L/|\ddot{\beta}_0|L_D \approx |\dddot{\beta}_0|L/\delta t_{\rm opt}^3$. In our simulated system, $\delta t_{\rm opt} \approx 1$ ps. The input repetition frequency was fixed again to achieve self-imaging with $N = 1$, i.e., $f_m = 4.4603$ GHz. The cross-correlation curves in Fig. 4 were calculated assuming an output microwave bandwidth of 100 GHz (input microwave bandwidth of 20 GHz or time width of each triangular pulse of 100 ps). Different cases were considered: 1) An identical second-order dispersion coefficient is introduced by the two dispersive lines in the system (solid curve); 2) second-order dispersion is only present in one of the two dispersive lines, namely, the input dispersive line (dashed curve) or the output dispersive line (dotted curve); and 3) the two dispersive lines introduce a second-order dispersion with the same magnitude but opposite signs (dashed-dotted curve). Fig. 4 shows that the presence of second-order dispersion in any of the two dispersive fibers will affect the system performance in a very similar fashion (compare dashed and dotted curves). In fact, as shown by the solid curve, when second-order dispersion is present in the two fibers, its effect is additive so that a higher deviation is induced in the output waveform (assuming that the second-order dispersion coefficients in the two fibers are of the same sign). In any case, Fig. 4 shows that as expected, the effect of second-order dispersion is only significant for fiber sections longer than the so-called second-order dispersion length

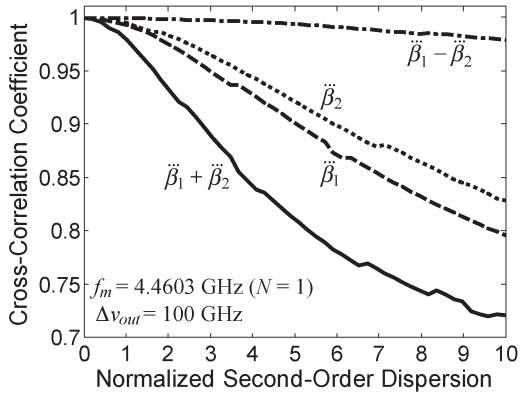

Fig. 4. Results from numerical simulations of the same microwave frequency upshifting system as in Fig. 3 but assuming the presence of second-order dispersions: Cross-correlation coefficient as a function of the normalized second-order dispersion term (see definition in the text), assuming that 1) an identical second-order dispersion coefficient is introduced by the two dispersive lines in the system (solid curve); 2) second-order dispersion is only present in one of the two dispersive lines, namely, the input dispersive line (dashed curve) or the output dispersive line (dotted curve); and 3) two dispersive lines introduce a second-order dispersion with the same magnitude but opposite signs (dashed-dotted curve). In these simulations, the input repetition frequency and output microwave bandwidth were fixed to $f_m = 4.4603$ GHz and $\Delta\nu_{\rm out} = 100$ GHz, respectively.

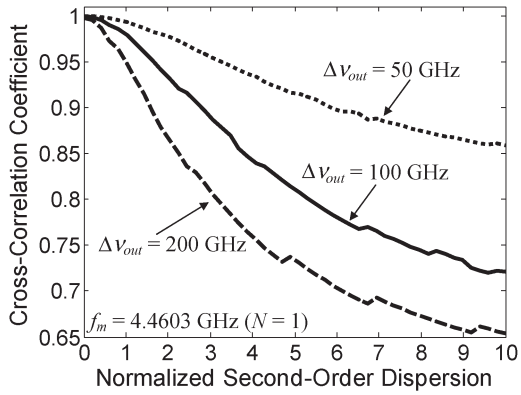

Fig. 5. Results from numerical simulations of the same microwave frequency upshifting system as in Fig. 4. Cross-correlation coefficient as a function of the normalized second-order dispersion term (see definition in the text), evaluated for different output microwave bandwidths, namely, 50 GHz (dotted curve), 100 GHz (solid curve), and 200 GHz (dashed curve). The input repetition frequency was fixed to $f_m = 4.4603$ GHz.

(for the input optical bandwidth). Another interesting finding is that the second-order dispersion effects can be compensated by using dispersive fibers with second-order dispersions of opposite signs; in particular, Fig. 4 shows that the second-order dispersion-induced distortion can be almost completely cancelled out if the two dispersive fibers introduce a second-order dispersion coefficient of the same magnitude but opposite sign (see dashed-dotted curve), even for fiber sections significantly longer than the characteristic second-order dispersion length.

Fig. 5 presents the cross-correlation curve evaluated as a function of the normalized second-order dispersion (assuming as the worst case the presence of second-order dispersion of the same sign in the two fibers) and for different input (output) microwave bandwidths. In particular, the cross-correlation curve was calculated for an output bandwidth of 50 GHz (dotted curve), 100 GHz (solid curve, same as in Fig. 4), and 200 GHz

(dashed curve). Fig. 5 shows that the second-order dispersion-induced distortion in the output waveform depends on the bandwidth of the synthesized signal, and in particular, a more significant distortion is observed when a broader bandwidth is synthesized. In other words, the microwave frequency upshifting system is more robust to second-order dispersion when used to synthesize a waveform with a narrower bandwidth.

As a general conclusion, we emphasize that the second-order dispersion-induced distortion can be minimized by ensuring that the used fiber sections are shorter than (or of the order of) the second-order dispersion length for the used optical bandwidth. Assuming an optical bandwidth of a few terahertz and a conventional SMF-28 fiber ($|\ddot{\beta}_0| \approx 0.1$ ps^3/km, at 1550 nm), this condition limits the fiber length to a few kilometers, which in turn may notably constraint the design flexibility provided by the system to achieve a large time–bandwidth product. However, in practice, the two dispersive lines in the system are typically implemented using a section of conventional fiber, SMF-28 (negative first-order dispersion), and a section of dispersion-compensating fiber (DCF, positive first-order dispersion) [1], [7]. The second-order dispersion terms in these two fibers are generally of opposite sign, thus making this conventional configuration more robust to second-order dispersion effects (the second-order dispersion effects in this case will be at least partially compensated; see the results in Fig. 4). If ultrabroadband operation over very large temporal apertures is desired, customized dispersive elements with reduced higher order dispersion coefficients could be used instead of conventional optical fibers. An attractive solution is that of chirped fiber Bragg gratings, which can be designed to almost completely remove higher order dispersion terms over very broad bandwidths [15], [16]. As an additional advantage, chirped fiber Bragg gratings can provide very high dispersions in significantly more compact forms than conventional optical fibers.

V. Proof-of-Concept Experiments

A. Frequency Upshifting of Microwave Tones

Experiments demonstrating frequency upshifting of microwave tones based on temporal self-imaging were reported in [7]. For completeness, we describe here in detail the main results of these experiments.

Fig. 6 shows a schematic of our experimental setup. An erbium-doped fiber ring laser (EDFRL) was used as the optical pulse source. The passive mode locking of the laser was achieved through nonlinear polarization rotation in a unidirectional ring resonator [17]. This source was operated at a wavelength of around 1550 nm and generated $\approx$ 1-ps optical pulses (full-width at half-maximum (FWHM) optical bandwidth $\approx$ 720 GHz, corresponding to a *total* bandwidth of $\approx$ 1.9 THz). The pulse repetition rate was set to 10 MHz by carefully adjusting the laser resonator length using a tunable delay line. Part of the laser radiation was coupled out by an optical coupler (C1), and after detection by PD1 and proper RF amplification (RFA), it was used as the synchronization signal (Synch.) in the RF synthesizer (Synth.) and as the triggering

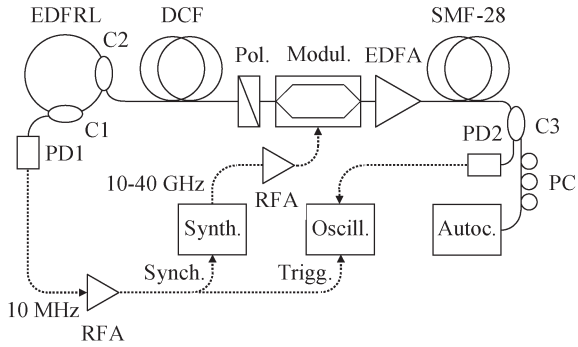

Fig. 6. Experimental setup with the notation given in the text.

(Trigg.) signal in the sampling oscilloscope (Oscill.). The fiber laser pulses were coupled out by a second optical coupler (C2) and subsequently stretched by the first dispersive stage (DCF, providing a total dispersion of $\ddot{\beta}_1 L_1 = +2153$ ps^2) to a time width of $\approx$ 9 ns (system's temporal aperture). After suitable polarization control with an optical polarizer (Pol.), the stretched pulses were temporally modulated in intensity by the amplified sinusoidal microwave voltage from the RF synthesizer using a Mach–Zehnder EO modulator (Modul.). The optical signal after modulation was temporally compressed using a second dispersive stage (conventional telecommunication fiber SMF-28). In our first set of experiments, SMF-28 introduced a dispersion of $\ddot{\beta}_2 L_2 = -1722$ ps^2. According to (4), this dispersion should provide a temporal magnification of $M_t = 0.2$, i.e., microwave frequency upshifting by $1/M_t = 5$. The microwave signal at the output of the second dispersive stage was extracted using a high-speed PD2 (bandwidth of 50 GHz) and measured with a sampling oscilloscope (bandwidth of 50 GHz).

Fig. 7 shows the measured signals at the output of the second dispersive stage (output of the system) when the frequency f_m of the input tone was fixed at different values (always around 10 GHz) to satisfy (9) with N varying from 4 to 6 in increments of 0.5. Specifically, the input frequencies were fixed to (a) $f_m = 8.600$ GHz $(N = 4)$; (b) $f_m = 9.120$ GHz $(N = 4.5)$; (c) $f_m = 9.610$ GHz $(N = 5)$; (d) $f_m = 10.080$ GHz $(N = 5.5)$; and (e) $f_m = 10.530$ GHz $(N = 6)$. As shown by the results in Fig. 7, a nearly ideal frequency upshifting process is always achieved when the self-imaging condition in (9) is satisfied with N being an *exact integer*. This is the case in Fig. 7 (a), (c), and (e). In these cases, our system provided a focused temporal replica of the original tone compressed by a factor of approximately $1/M_t = 5$, i.e., the desired microwave frequency upshifting by a factor of $\approx$ 5 was achieved. In particular, the frequencies of the output tones (as estimated from Fourier analysis of the experimental curves) were (a) $\approx$ 42.820 GHz, (c) $\approx$ 47.874 GHz, and (e) $\approx$ 52.046 GHz (frequency upshifting by 4.979, 4.982, and 4.943, respectively), and the corresponding cross-correlation coefficients C between the measured input and output waveforms [as defined in (16)] were estimated as (a) 0.95, (c) 0.95, and (e) 0.93. As expected for an experimental realization, the estimated cross-correlation coefficients from measurements are slightly lower than those theoretically

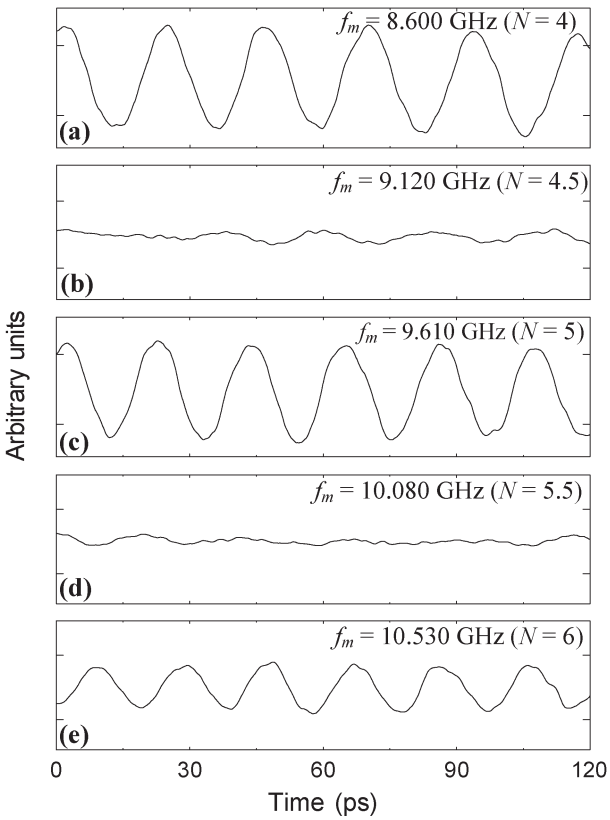

Fig. 7. Measured microwave signals at the output of the microwave frequency upshifting system (compression factor of $1/M_t = 5$) for input RF tones of different frequencies (f_m around 10 GHz).

predicted (see Fig. 2). When N was not an integer, the amplitude of the output signal decreased drastically; see, for instance, the results in Fig. 7(b) and (d), in which the microwave signals were practically filtered out by the TI system and essentially only noise was received at the output. The cross-correlation coefficients could not be easily estimated in these two cases since it is not evident to establish an objective criterion for temporally synchronizing the measured noisy output waveforms and the input tones (as required for the calculation of these coefficients). Nonetheless, the presented results clearly show that the simplified TI system used in our experiments would be unable to generate frequencies as high as those demonstrated here (around 50 GHz) unless the system is designed and configured to exploit the temporal self-imaging effect.

To further illustrate the capabilities of the proposed microwave frequency upshifting approach, we conducted a series of experiments to obtain radiation at frequencies well above 100 GHz. Fig. 8 shows the measured temporal signals at the input (top plot) and at the output (bottom) of the second dispersive stage (SMF-28) when the input frequency was fixed to $f_m = 39.870$ GHz to satisfy (9) with $N = 86$. The bandwidth of our time-domain measurement system (PD2 + oscilloscope) was now insufficient to capture the output temporal waveform, and as a result, the signals in these experiments were measured using an optical autocorrelator (Autoc. in Fig. 6). In the results shown in Fig. 8, the output signal exhibited a frequency of $f_{\text{out}} \approx 199.35$ GHz (determined by Fourier analysis), i.e., the predicted frequency upshifting by 5 was achieved. Specifically,

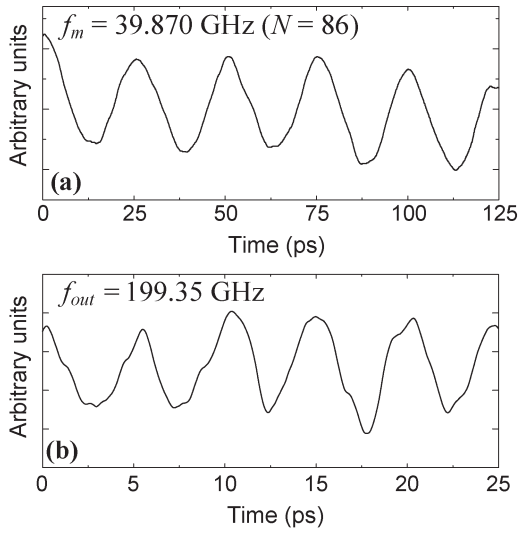

Fig. 8. Autocorrelation traces corresponding to the optical signals measured (a) before and (b) after the second dispersive stage in the microwave frequency upshifting system when the system is configured for achieving a compression factor of $1/M_t = 5$ with $f_m = 39.870$ GHz.

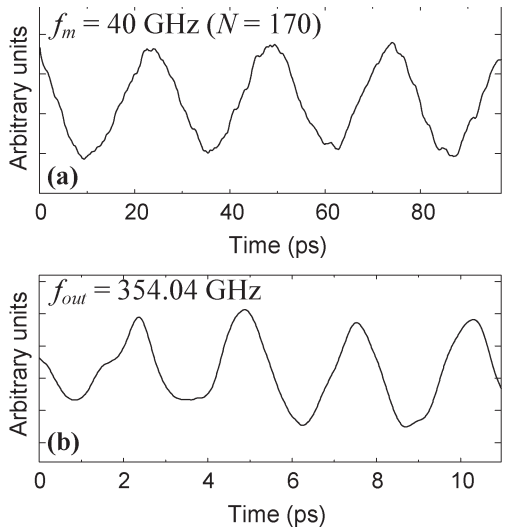

Fig. 9. Autocorrelation traces corresponding to the optical signals measured (a) before and (b) after the second dispersive stage in the microwave frequency upshifting system when the system is configured for achieving a compression factor of $1/M_t = 8.85$ with $f_m = 40$ GHz.

we estimated a cross-correlation coefficient between the measured input and output autocorrelation traces of ≈ 0.89. A larger frequency upshifting factor was finally achieved using a longer section of SMF-28 fiber at the second dispersive stage (total dispersion of $\ddot{\beta}_2 L_2 = -1910$ ps^2). According to (4), this system should provide a microwave frequency upshifting by $1/M_t = 8.85$. Fig. 9 shows the measured temporal signals at the input (top plot) and at the output (bottom) of the second dispersive stage (SMF-28) when the input frequency was fixed to $f_m = 40$ GHz to satisfy (9) with $N = 170$. The output signal exhibited a frequency of 354.04 GHz (determined by Fourier analysis), thus demonstrating the expected frequency upshifting by exactly 8.85. In this case, we estimated a cross-correlation coefficient between the measured input and output autocorrelation traces of ≈ 0.94. Again, the cross-correlation

coefficients between the measured input and output waveforms in this last set of experiments are slightly lower than those theoretically expected (see Fig. 3). In particular, the observed distortions in the measured temporal waveforms in Figs. 8 and 9 are in part associated with the instabilities in the autocorrelation measurement system.

For comparison, the reader can easily prove from (7) that if the temporal Talbot effect had not been exploited, the maximum achievable frequency (using the same configuration and parameters as in our examples here) would have been limited to $\approx$ 10–15 GHz. This again shows the drastically superior performance that can be achieved by properly exploiting the temporal Talbot effect in a microwave frequency upshifting system.

VI. Summary and Conclusion

In conclusion, a fiber-based microwave frequency upshifting technique for broadband AWG has been analyzed in detail. This study follows previously reported experimental results on this technique. In a microwave frequency upshifting scheme, a low-frequency arbitrary microwave signal is temporally compressed into a high-frequency replica using a simple and practical fiber-based system. The focus of our paper is on the so-called Talbot-based approach, in which the microwave signal to be frequency upshifted is a (quasi-)periodic temporal waveform. This includes nonmodulated or slowly (amplitude and/or phase) modulated microwave tones, or in general, any given arbitrary periodic waveform. The design specifications of a Talbot-based microwave frequency upshifting system have been derived and the practical capabilities and limitations of these systems have been investigated both analytically and numerically. Our theoretical findings and numerical simulations are in very good agreement. The results reported here show the superior performance associated with the use of the temporal Talbot effect in a microwave frequency upshifting system and have also allowed us to clearly establish the actual capabilities and constraints of this approach for broadband AWG. Specifically, it has been shown that electrical (microwave) frequencies up to a few hundreds of gigahertz over nanosecond temporal windows can be easily obtained with the proposed technique using pulsed optical sources providing optical bandwidths in the terahertz range. In practice, the achievable electrical bandwidth may be limited by the output PD bandwidth. A numerical analysis of the influence of higher order effects, in particular second-order dispersions in the fibers, has also been conducted. This analysis reveals the need for minimizing the second-order dispersion terms in the used fibers to avoid a significant distortion in the synthesized waveforms. The influence of second-order dispersion is especially detrimental for synthesizing ultrabroadband waveforms. Simple design rules have been given to avoid these detrimental effects in a practical system.

Appendix

In the analysis of the system in Fig. 1, we assume an ultrashort Gaussian input optical pulse. After propagation through the first dispersive fiber (total dispersion $\ddot{\beta}_1 L_1$), this pulse is temporally broadened and chirped. In particular, assuming that the input dispersion is sufficiently high, the complex envelope of the pulse at the fiber output can be expressed as

$$u\left(t, L_1^-\right) = \exp\left(-\left(\frac{t}{\tau_1}\right)^2\right) \exp\left(j\frac{t^2}{2\ddot{\beta}_1 L_1}\right) \tag{A1}$$

with $\tau_1 \approx \ddot{\beta}_1 L_1 \Delta\omega_{\text{opt}}$, where $\Delta\omega_{\text{opt}}$ is the input optical bandwidth. We note again that in our analysis the time delays introduced by the different elements in the system (i.e., dispersions and EO modulator) are not considered. The chirped pulse is then intensity modulated in an EO modulator (e.g., Mach–Zehnder intensity modulator) by the input electrical (microwave) signal $V_{\text{in}}(t)$. Assuming that the modulation depth is sufficiently small to ensure linear modulation operation, the optical signal at the output of the EO modulator can be written as

$$u\left(t, L_1^+\right) = u\left(t, L_1^-\right)\left[1 + aV_{\text{in}}(t)\right] = V'(t) \exp\left(j\frac{t^2}{2\ddot{\beta}_1 L_1}\right) \tag{A2}$$

where $V'(t) = \exp(-[t/\tau_1]^2)[1 + aV_{\text{in}}(t)]$. This optical signal is dispersed again in a second dispersive fiber providing a total dispersion $\ddot{\beta}_2 L_2$. The temporal waveform after dispersion can be calculated as $u(t, L_1 + L_2) = u(t, L_1^+) * h_2(t)$, where the asterisk denotes convolution, and $h_2(t)$ is the temporal impulse response of the fiber dispersive medium $h_2(t) \propto \exp(jt^2/(2\ddot{\beta}_2 L_2))$. The convolution operation can be developed as

$$\begin{aligned} u(t, L_1 + L_2) &= u\left(t, L_1^+\right) * h_2(t) \\ &\propto \exp\left(j\frac{t^2}{2\ddot{\beta}_2 L_2}\right) \int_{-\infty}^{+\infty} V'(\tau) \exp\left(j\frac{\tau^2}{2\alpha}\right) \\ &\quad \times \exp\left(-j\frac{t\tau}{\ddot{\beta}_2 L_2}\right) d\tau \end{aligned} \tag{A3}$$

where $1/\alpha = (1/\ddot{\beta}_1 L_1) + (1/\ddot{\beta}_2 L_2)$. The last integral in (A3) can be solved by considering the term $\exp(-jt\tau/\ddot{\beta}_2 L_2)$ as the kernel of a Fourier integral

$$\begin{aligned} &\int_{-\infty}^{+\infty} V'(\tau) \exp\left(j\frac{\tau^2}{2\alpha}\right) \exp\left(-j\frac{t\tau}{\ddot{\beta}_2 L_2}\right) d\tau \\ &\qquad = \Im\left\{V'(\tau) \exp\left(j\frac{\tau^2}{2\alpha}\right)\right\}_{\omega = \frac{t}{\ddot{\beta}_2 L_2}} \end{aligned} \tag{A4}$$

where the symbol $\Im$ holds for Fourier transform. Using the product–convolution property of the Fourier integral, we obtain

$$\begin{aligned} \Im\left\{V'(\tau) \exp\left(j\frac{\tau^2}{2\alpha}\right)\right\} &\propto \widetilde{V}'(\omega) * \exp\left(-j\alpha\frac{\omega^2}{2}\right) \\ &= \exp\left(-j\alpha\frac{\omega^2}{2}\right) \int_{\Delta\Omega} \widetilde{V}'(\Omega) \exp\left(-j\alpha\frac{\Omega^2}{2}\right) \exp(j\alpha\omega\Omega)\, d\Omega \end{aligned} \tag{A5}$$

where $\widetilde{V}'(\omega) = \Im\{V'(\tau)\}$ and $\Delta\Omega$ is the total spectral bandwidth of $V'(t)$ $[\widetilde{V}'(\omega)]$. If this bandwidth is sufficiently narrow so that

$$|\alpha|\frac{\Delta\Omega^2}{8} \ll \pi \tag{A6}$$

then the phase term $\exp(-j\alpha\Omega^2/2)$ in the integral of (A5) can be neglected and results in

$$\Im\left\{V'(\tau)\exp\left(j\frac{\tau^2}{2\alpha}\right)\right\} \propto \exp\left(-j\alpha\frac{\omega^2}{2}\right)V'(\tau=\alpha\omega). \tag{A7}$$

Introducing (A7) into (A4), we obtain

$$\int_{-\infty}^{+\infty} V'(\tau)\exp\left(j\frac{\tau^2}{2\alpha}\right)\exp\left(-j\frac{t\tau}{\ddot{\beta}_2 L_2}\right)d\tau = \exp\left(-j\frac{t^2}{2M_t(\ddot{\beta}_2 L_2)}\right)V'\left(\tau=\frac{t}{M_t}\right) \tag{A8}$$

with

$$M_t = \frac{\ddot{\beta}_2 L_2}{\alpha} = 1 + \frac{\ddot{\beta}_2 L_2}{\ddot{\beta}_1 L_1}. \tag{A9}$$

Introducing the result from (A8) into (A3), we finally derive

$$u(t, L_1+L_2) \propto \exp\left(j\frac{t^2}{2(\ddot{\beta}_1 L_1)M_t}\right)V'\left(\tau=\frac{t}{M_t}\right). \tag{A10}$$

The signal received at the output of the PD $V_{\rm out}(t)$ is proportional to the average intensity of this optical signal and results in

$$V_{\rm out}(t) \propto |u(t, L_1+L_2)|^2 \propto \left|V'\left(\tau=\frac{t}{M_t}\right)\right|^2 \approx \exp\left(-2\left(\frac{t}{M_t\tau_1}\right)^2\right)\left[1+2aV_{\rm in}\left(\frac{t}{M_t}\right)\right]. \tag{A11}$$

It should be mentioned that a similar expression to that in (A11) has been obtained for temporal stretching systems assuming an ideal electrical tone (sinusoidal waveform) as the input electrical signal [2]. Our analysis here is more general and valid for any given *arbitrary* input electrical waveform.

REFERENCES

[1] J. U. Kang, M. Y. Frankel, and R. D. Esman, "Demonstration of microwave frequency shifting by use of a highly chirped mode-locked fiber laser," *Opt. Lett.*, vol. 23, no. 15, pp. 1188–1190, Aug. 1998.

[2] F. Coppinger, A. S. Bhushan, and B. Jalali, "Photonic time stretch and its application to analog-to-digital conversion," *IEEE Trans. Microw. Theory Tech.*, vol. 47, no. 7, pp. 1309–1314, Jul. 1999.

[3] T. Yilmaz, C. M. DePriest, T. Turpin, J. H. Abeles, and P. J. Delfyett, "Toward a photonic arbitrary waveform generator using a mode-locked external cavity semiconductor laser," *IEEE Photon. Technol. Lett.*, vol. 14, no. 11, pp. 1608–1610, Nov. 2002.

[4] J. Chou, Y. Han, and B. Jalali, "Adaptive RF-photonic arbitrary waveform generator," *IEEE Photon. Technol. Lett.*, vol. 15, no. 4, pp. 581–583, Apr. 2003.

[5] O. Levinson and M. Horowitz, "Generation of complex microwave and millimeter-wave pulses using dispersion and Kerr effect in optical fiber systems," *J. Lightw. Technol.*, vol. 21, no. 5, pp. 1179–1187, May 2003.

[6] J. D. McKinney, D. Seo, D. E. Leaird, and A. M. Weiner, "Photonically assisted generation of arbitrary millimeter-wave and microwave electromagnetic waveforms via direct space-to-time optical pulse shaping," *J. Lightw. Technol.*, vol. 21, no. 12, pp. 3020–3028, Dec. 2003.

[7] J. Azaña, N. K. Berger, B. Levit, V. Smulakowsky, and B. Fischer, "Frequency shifting of microwave signals by use of a general temporal self-imaging (Talbot) effect in optical fibers," *Opt. Lett.*, vol. 29, no. 24, pp. 2849–2851, Dec. 2004.

[8] Y. Han and B. Jalali, "Time–bandwidth product of the photonic time-stretched analog-to-digital converter," *IEEE Trans. Microw. Theory Tech.*, vol. 51, no. 7, pp. 1886–1892, Jul. 2003.

[9] W. J. Caputi, "Stretch: A time-transformation technique," *IEEE Trans. Aerosp. Electron. Syst.*, vol. AES-7, no. 2, pp. 269–278, Mar. 1971.

[10] J. M. Fuster, D. Novak, A. Nirmalathas, and J. Marti, "Single sideband modulation in photonic time-stretched analogue-to-digital conversion," *Electron. Lett.*, vol. 37, no. 1, pp. 67–68, Jan. 2001.

[11] J. Azaña and L. R. Chen, "General temporal self-imaging phenomena," *J. Opt. Soc. Amer. B, Opt. Phys.*, vol. 20, no. 7, pp. 1447–1458, Jul. 2003.

[12] B. H. Kolner and M. Nazarathy, "Temporal imaging with a time lens," *Opt. Lett.*, vol. 14, no. 12, pp. 630–632, 1989.

[13] C. V. Bennet and B. H. Kolner, "Upconversion time microscope demonstrating 103× magnification of femtosecond waveforms," *Opt. Lett.*, vol. 24, no. 11, pp. 783–785, Jun. 1999.

[14] H. Ito, S. Kodama, Y. Muramoto, T. Furuta, T. Nagatsuma, and T. Ishibashi, "High-speed and high-output InP-InGaAs unitraveling-carrier photodiodes," *IEEE J. Sel. Topics Quantum Electron.*, vol. 10, no. 4, pp. 709–727, Jul./Aug. 2004.

[15] J. Azaña and M. A. Muriel, "Temporal self-imaging effects: Theory and application for multiplying pulse repetition rates," *IEEE J. Sel. Topics Quantum Electron.*, vol. 7, no. 4, pp. 728–744, Jul.–Sep. 2001.

[16] P. C. Chou, H. A. Haus, and J. F. Brennan, III, "Reconfigurable time-domain spectral shaping of an optical pulse stretched by a fiber Bragg grating," *Opt. Lett.*, vol. 25, no. 8, pp. 524–526, Apr. 2000.

[17] K. Tamura, J. Jacobson, E. P. Ippen, H. A. Haus, and J. G. Fujimoto, "Unidirectional ring resonators for self-starting passively mode-locked lasers," *Opt. Lett.*, vol. 18, no. 3, pp. 220–222, Feb. 1993.

José Azaña (M'03) was born in Toledo, Spain, on December 8, 1972. He received the Ingeniero de Telecomunicación degree and the Ph.D. degree in optical signal processing and fiber Bragg gratings from the Universidad Politécnica de Madrid, Madrid, Spain, in 1997 and 2001, respectively. He completed part of his Ph.D. work at the University of Toronto, Toronto, ON, Canada, and at the University of California, Davis.

From September 2001 to mid 2003, he was a Postdoctoral Research Associate with the Department of Electrical and Computer Engineering, McGill University, Montreal, QC, Canada. He recently joined the Institut National de la Recherche Scientifique, Montreal, where he is a Research Professor with the "Ultrafast Optical Processing" group. His research work has resulted in more than 50 publications in top scientific and engineering journals and has been recognized with several distinctions in Spain and Canada. His current research interests focus on fiber and integrated technologies for ultrafast optical signal processing and optical pulse shaping, for various applications, including optical telecommunications, ultrafast metrology, biomedical imaging, and microwave waveform manipulation.

Prof. Azaña is a member of the Optical Society of America.

Naum K. Berger received the M.S. degree in physics from the Novosibirsk State University, Novosibirsk, Russia, in 1967 and the Ph.D. degree in physical electronics (including quantum electronics) from the Institute of Automatics and Electrometry, Novosibirsk, in 1978.

During 1970–1993, he was a Senior Lecturer, a Professor at the Physics Department, and the Head of the Department of Electrical Engineering at the Khabarovsk State Technical University, Khabarovsk, Russia. Since 1995, he has been a Research Associate with the Technion—Israel Institute of Technology, Haifa, Israel. His research interest is in fiber optics, optical pulse processing and characterization, and fiber Bragg gratings.

Boris Levit received the M.S. degree in physics from the Ural State Technological University, Ekaterinburg, Russia, in 1972 and the Ph.D. degree in the autodyne effect in gas and diode lasers from the Moscow State Pedagogical University, Moscow, Russia, in 1982.

Since 1997, he has been a Research Associate in the Electro-Optics Laboratory, the Technion—Israel Institute of Technology, Haifa, Israel. His research interests include experimental study of semiconductor and fiber lasers, fiber Bragg gratings, and characterization of ultrashort optical pulses. He has over 40 publications and patents.

Baruch Fischer received the Ph.D. degree from Bar Ilan University, Ramat-Gan, Israel, in 1980.

He then joined the Technion—Electrical Engineering Department, Haifa, Israel, where he is currently a Max Knoll Professor in electrooptics and electronics. In the early 1980s, he was among the founders of the research field of nonlinear photorefractive optics, contributing to the basic wave mixing formalism, the inventions of the first self-pumped phase conjugators, the double phase conjugation, and the first steps in the study of photorefractive self-defocusing and self-trapping and photorefractive solitons. Later, he contributed to the study of nonlinear effects in bacterio-rhodopsin and fiber optics. He was the Head of the Technion Micro-Electronics Research Center, from 1993 to 2001, and the Dean from 1999 to 2004. Since 1999, he has also been the Director of the board of MRV-Communications Inc., Chatsworth, CA. His research interest is in nonlinear optics, fiber optics, pulse optics, statistical-mechanics and quantum-mechanics-based study in optics and lasers, and short pulse physics. The latter subject includes a new statistical–mechanics approach to understand the many interacting lightwave modes in lasers, mostly relevant to pulse formation in mode-locked lasers. This study shows, for example, a thermodynamic-like "melting–freezing" pathway and critical behavior of pulses in mode-locked lasers (similar to gas–liquid–solid and ferromagnetic phase transitions), explaining, predicting, and observing many exciting features of pulse lasers.

Prof. Fischer is a Fellow of the Optical Society of America. From 1981 to 1983, he was a Weizmann Post-Doctorate Fellow at the California Institute of Technology, Pasadena. He was a Topical Editor for *Optics Letters* from 1996 to 2002 and is on the Editorial Board of the *International Journal of Nonlinear Optical Physics and Materials* since 1992.